A Quantum Contention
Study of the Competition between
Antiferromagnetism and Singlet Formation on a
Quasicrystal Lattice.

Nicole Hartman[1]
Mentor: Dr. Richard Scalettar[2]

[1]   *Southern Methodist University, Dallas, Texas 75275 USA*
[2]   *University of California at Davis, Davis, CA 95616 USA*

E-mail: nhartman@smu.edu, scalettar@physics.ucdavis.edu

ABSTRACT:

Motivated by experimental discovery of quantum antiferromagnetism (AF) in quasicrystal (QC) materials such as Au-Al-Yb compounds [1], we wanted to examine these studies on quasicrystalline approximates [2, 3]. To differentiate the effects due to the non-periodic structure and the varying coordination number, we repeated the analysis for two different structures, a Lieb lattice with periodicity but varying coordination, and the quasicrystal structure which is not periodic. Studying the spin-spin correlation function around this phase transition gives an estimate for $V_c = 0.9$ at $\beta = 20$.
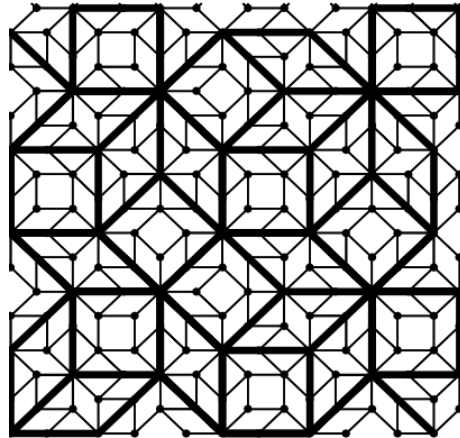
Contents

1 Introduction

Variation of the systems parameters facilitates the study of the phase transition between antiferromagnetism and singlet formation on a lattice. This phenomenon has been extensively studied using determinant Monte Carlo techniques on periodic lattices, such as the 1D, 2D, and 3D square lattices [4]. However, recent experimental results have revealed that this phenomenon is not confined to periodic lattices, as the quasicrystal material Au-Al-Yb also revealed antiferromagnetic ordering [1]. Therefore, we were motivated to explain these experimental results using the Hubbard model [6]. Our collaborators had some tables detailing the site bonds for QCs on a couple of different sized lattices. Although the quasicrystalline approximates did display antiferromagnetism, they failed to reproduce another interesting property, non-Fermi liquid behavior [5]. Therefore, one must be cautious in applying the results from this study since it does not reproduce all of the physics. To

explain this project, I will start by explaining a bit more about quasicrystals, the experimental material we were attempting to model, and the phenomenon of antiferromagnetism versus singlet formation. Then I will explain the Periodic Anderson Model Hamiltonian that encodes the physics, the methods of this analysis, and conclude with our results.

1.1 Quasicrystals

Colloquially, a *crystal* is considered a periodic structure formed by repeated application of a unit cell. Many materials in nature do possess this long range periodic order and we can take the Fourier transform of a periodic lattice and study the reciprocal lattice to more easily gain information about the density of states and allowed energies of the system. A more inclusive definition of a crystal, can help diversify the physics that we are able to study using similar techniques. A *quasicrystal* is a structure that is ordered, but not periodic as it does *not* possess a translational symmetry. A picture of the 2D quasicrystal that I was working with is shown in the figure below [2].

This picture encodes the information for two 2D lattices, where the bold black lines show the bonds for a 41 site lattice, and the skinnier lines show the connections for a 239 site lattice. Larger structures are formed not by repeating a unit cell, but rather by a process known as *inflation*. In the figure, you can see that the solid lines form squares and parallelograms, and the larger lattice was created by implementing a smaller structure inside the larger one, similar to how fractals are created.

To study the physics of how these atoms interact with each other, recall that in quantum mechanics two atoms interact with each other through the overlap of their wavefunctions, as shown in Fig. 2. The wavefunction is solved for the hydrogen atom using *separation of variables*, where the wavefunction, ψ_{nlm}, is written as the product of the radial and angular terms.

Figure 1: The thick lines show the bonds for the 41 site lattice while the thin lines show how the 41 site lattice can be *inflated* to form the 239 site lattice [2].

$$\psi_{nlm}(r,\theta,\phi) = R_{nl}(r)Y_{lm}(\theta,\phi) \tag{1.1}$$

$R_{nl}(r,\theta)$ is a product of the exponential and Laguerre polynomials and $Y_{lm}(\theta,\phi)$ are the spherical harmonics [8]. The radial dependence depends on the principle quantum number, n, as

$$R_{nl}(r) \propto \exp\left(-\frac{r}{na_0}\right) \tag{1.2}$$
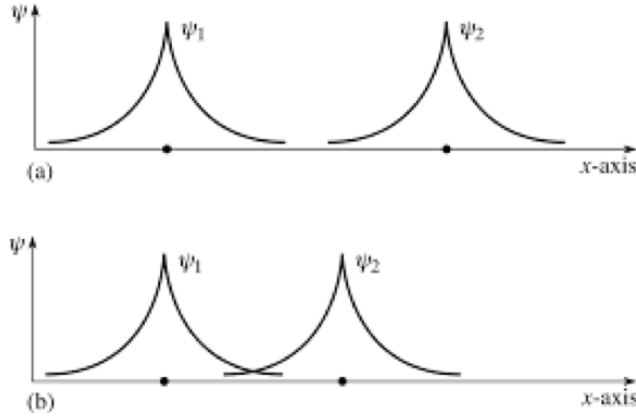
Figure 2: The overlap between atomic wavefunctions characterizes interactions[7]

where a_0 is the Bohr radius. As n increases, R_{nl} increases, so the expectation value of r is larger for bigger n. This qualitative result carries over to larger Z elements as well. The valence electrons for Au, Al, and Yb are in $5d$, $3p$, and $4f$ orbitals, respectively, so this implies that the Au atoms have a more dispersed wavefunction than Al or Yb. The $3p$ and $4f$ orbitals will both have a negligible range compared with that of the $5d$ orbital, so we can generalize by denoting conduction orbitals by as d and the localized orbitals as f. This notation holds for general quasicrystals as well since most include both a transition metal and a Lanthanide. Then with this approximation, we have two wavefunctions, ψ_d and ψ_f corresponding to the *conduction* and *localized* orbitals, respectively. Then we can define the energy required to hop between sites using the kinetic energy operator $\hat{T}$

$$t = \int_{-\infty}^{\infty} \psi_d^* \hat{T} \psi_d dx \qquad V = \int_{-\infty}^{\infty} \psi_d^* \hat{T} \psi_f dx \qquad 0 = \int_{-\infty}^{\infty} \psi_f^* \hat{T} \psi_f dx \qquad (1.3)$$

where t is the energy to hop between two conduction sites and V is the energy to hop between a conduction and localized site. Because of the negligible overlap between orbitals of localized sites, the hopping energy between two f orbitals is zero.
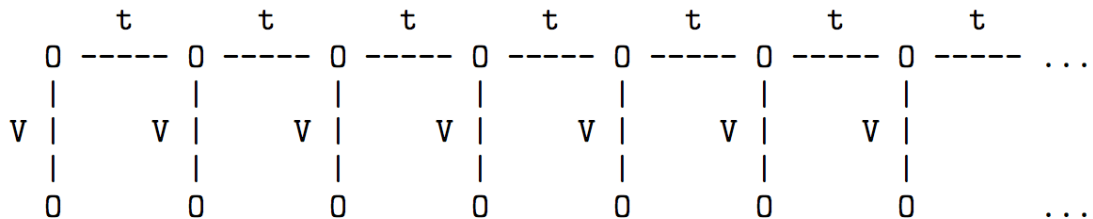
Figure 3: Illustration for how a 1D chain can have a localized site added at each conduction site, as specified by the Periodic Anderson Model [6]

Modeling a crystal in this way defines the *Periodic Anderson Model* (PAM) for a lattice. Figure 3 demonstrates this model if the conduction sites are connected together in a 1D chain, with a localized site below each of them. In this project, the conduction sites are
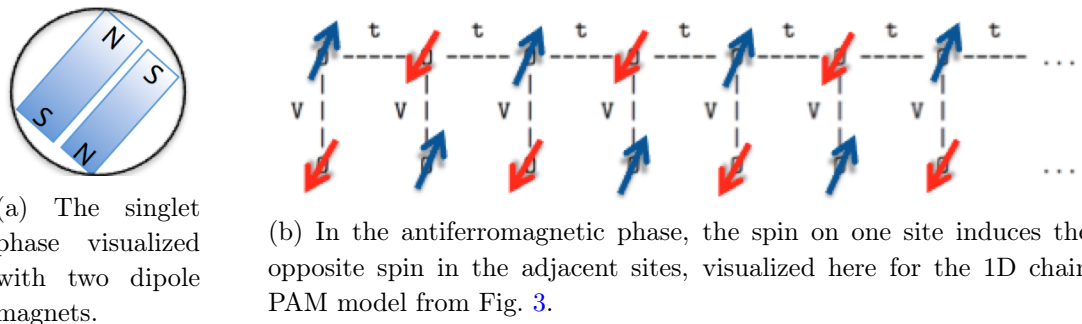
connected according to Fig. 1, and then each of these conduction sites has an associated localized site. So the "41 site" lattice actually has 82 orbitals, 41 conduction and 41 localized orbitals, and similarly for the 231 site lattice.

1.2 Antiferromagnetism vs. Singlet Formation

Now that the geometry has been described, we can investigate the physics processes under consideration.

If the connection between the localized and conduction sites, V, is strong enough, the conduction and localized orbitals will hybridize. After hybridization, the two electrons are in the *same* spatial wave-function, so that the Pauli exclusion principle requires that their spins must be oppositely aligned. This is analogous to the ground state of the hydrogen molecule when the two electrons are in the anti-symmetric state, a phenomenon known as singlet formation. Since the communication between the singlet and antiferromagnetic states is so strong, the two opposite spins orbitals effectively cancel each other out, allowing no long range ordering of the spins on the lattice. An analogous classical picture involves two magnetic dipoles canceling each other's magnetic fields, shown in Fig. 4a.

In the competing process, if the hopping energy V is not too strong, but comparable to the hopping energy t, the localized sites on the lattice will also be able to communicate with each other. An example of how this phenomenon can occur for the 1D PAM picture is displayed in Fig. 4b. The down spin on the lower right localized site makes it energetically favorable to have an up spin on the adjacent conducting site. This site then induces a down spin in the neighboring conduction sites, which induces an up spin on the adjacent localized sites. The pattern continues throughout the lattice, producing a system with magnetic ordering, but no net magnetization.

(a) The singlet phase visualized with two dipole magnets.

(b) In the antiferromagnetic phase, the spin on one site induces the opposite spin in the adjacent sites, visualized here for the 1D chain PAM model from Fig. 3.

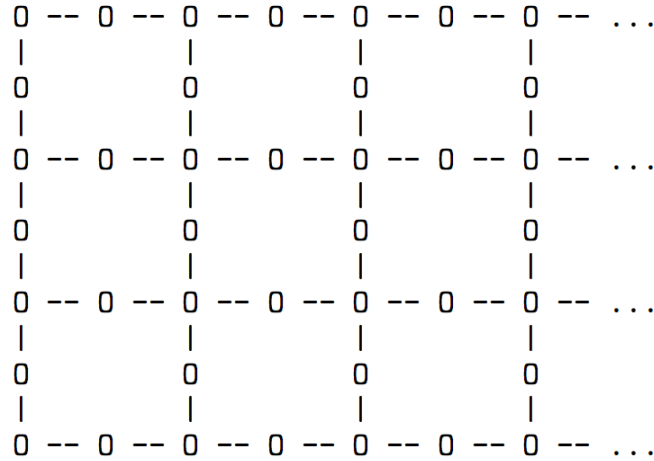**Figure 4**: Illustration of the two different "phases" for the electron spins in a crystal.

The system will transition from one of these states to the other through a phase transition governed by the hopping parameter V, as below some value V_c it becomes more energetically favorable for the system to become antiferromagnetic. At *half-filling*, the lattice has, on average, one electron per site. For a lattice to have a stable antiferromagnetic configuration at half-filling, each site with an up-spin electron needs to be adjacent to a site with a down spin electron, or bipartite. A *bipartite* lattice can be divided into two sublattices A and B where each site in sublattice A is surrounded by sites in sublattice B,

and vice versa. For example, the square, Lieb (Fig. 6), and hexagonal lattices are bipartite, while the triangular lattice is not.
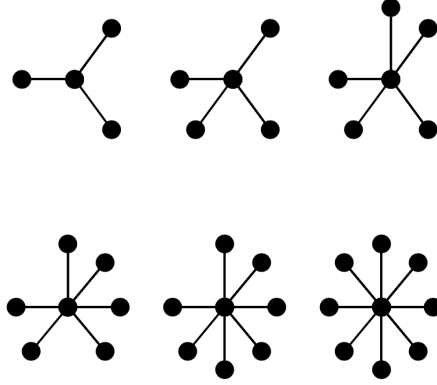
Figure 5: Orientation for the sites with the differing coordination numbers in the quasicrystal, ranging from $z = 3$ to 8, and named "Heisenberg stars" [2]

The quasicrystal lattice not only has no long range order, but also has varying coordination numbers, or different numbers of nearest neighbor bonds (see Fig. 1). We wanted to study the formation of antiferromagnetic ordering on the quasicrystal using a determinant Monte Carlo implementation for the Hubbard Model, something that has never been done before. To explore the differences for whether discrepancies from other implementations for the square lattice were due to the non-periodicity, or the differing coordination numbers (z), we also looked at the phase transition in the Lieb lattice, shown in Fig. 6, a bipartite structure that is periodic, but has differing coordination numbers ($z = 2$ and $z = 4$).

```
0 -- 0 -- 0 -- 0 -- 0 -- 0 -- 0 -- ...
|         |         |         |
0         0         0         0
|         |         |         |
0 -- 0 -- 0 -- 0 -- 0 -- 0 -- 0 -- ...
|         |         |         |
0         0         0         0
|         |         |         |
0 -- 0 -- 0 -- 0 -- 0 -- 0 -- 0 -- ...
|         |         |         |
0         0         0         0
|         |         |         |
0 -- 0 -- 0 -- 0 -- 0 -- 0 -- 0 -- ...
```

Figure 6: Illustration for the Lieb lattice [6]

2 Theory

The Hamiltonian incorporates this qualitative picture to describe quantitatively the physics that we are modeling. The quantities of interest in the Hamiltonian are written in terms of creation and destruction operators.

2.1 Creation and Destruction Operators

In an introductory quantum mechanics course, Schrodinger's equation for the simple harmonic oscillator can be solved in terms of creation and destruction operators, as successively higher energy states are reached by applying the creation operator to the wavefunction, and lower energy wavefunctions achieved by applying the destruction operator [8]. The lowest energy for the system is *ground state energy*, so applying the destruction operator to the ground state returned 0.

In a lattice, we use creation and destruction operators to create and destroy electrons on specified sites. The operator $d_{j\sigma}^\dagger$ creates a conduction electron with spin σ on the site j. Because of the Pauli exclusion principle, two electrons cannot occupy the same quantum state, so we cannot have two up-spin electrons on the same site. If you try to create another electron with the same spin at a site that already has an electron with this spin, you must get zero, exemplified by the equation below

$$d_{2\uparrow}^\dagger \ket{vac} = \ket{0 \uparrow 00\ldots} \qquad d_{2\uparrow}^\dagger \ket{0 \uparrow 00\ldots} = 0 \qquad (2.1)$$

where $\ket{0 \uparrow 00\ldots}$ denotes a lattice that is empty, except for a spin-up electron on site 2, and $\ket{vac}$ is the *vacuum state*, a completely empty lattice. The destruction operator for conduction sites, $d_{j\sigma}$, destroys a conduction electron at site j, or returns 0 if there is no conduction electron with spin σ on site j already.

$$d_{2\uparrow} \ket{0 \uparrow 00\ldots} = \ket{vac} \qquad d_{2\downarrow} \ket{0 \uparrow 00\ldots} = 0 \qquad (2.2)$$

Similarly, $f_{j\sigma}^\dagger$ and $f_{j\sigma}$ create and destroy, respectively, spin σ electrons in the *localized* orbital at site j. As before, the f denotes the localized orbital while d denotes the conduction orbital.

We can count the *number* of localized electrons of spin σ at site j by using the number operator $n_{j_f\sigma} = f_{j\sigma}^\dagger f_{j\sigma}$. When $n_{j_f\sigma}$ operates on a state, it returns the same state, multiplied by the eigenvalue defined by the number of localized spin σ electrons at site j.

2.2 The Hamiltonian

The Hamiltonian is the sum of the kinetic and potential energies, and Eq. (2.3) encodes the physics of this model using the creation and destruction operators

$$H = -t \sum_{\langle ij \rangle \sigma} d_{i\sigma}^\dagger d_{j\sigma} - V \sum_i \left(d_{i\sigma}^\dagger f_{i\sigma} + f_{i\sigma}^\dagger d_{i\sigma} \right) + U_f \sum_{i_f} \left(n_{i_f\uparrow} - \frac{1}{2} \right) \left(n_{i_f\downarrow} - \frac{1}{2} \right) \qquad (2.3)$$

where $\sum_{\langle ij \rangle}$ means sum over all nearest neighbor sites, i and j. From Section 1.1, t is the hopping energy between two conduction sites and V is the hopping energy between

a conduction and localized orbital. The first summation destroys the electron of spin σ at site i, and creates one at site j, and since i and j are neighboring sites, this shows an electron hopping between conduction sites. Similarly, the second summation has a term which destroys a localized electron at site i, and then creates one at the conduction site i, and another term that destroys a conduction electron at site i, and then creates one at the localized site i, characterizing an electron hopping between a localized and conduction site with hopping energy V. So the first two summations account for the kinetic energy.

The last summation places a potential U_f at the localized orbitals to induce local magnetic moments. There are four possible configurations that electrons can occupy a single site in, shown in Fig. 7. The factors of $\frac{1}{2}$ in the terms $\left(n_{i_f\uparrow} - \frac{1}{2}\right)$ and $\left(n_{i_f\downarrow} - \frac{1}{2}\right)$ allow the potential energies for the configurations to be centered about zero, which we are free to do because potentials can only be defined up to an arbitrary constant. A system tends to the state of lowest potential energy, so the configurations with energy $-U_f/4$ with only one electron at the site will be favored by including this term.


Figure 7: The potential induced on a localized site to induce local moments. The blue arrow denotes a spin up electron, while the red arrow denotes a spin down electron.

3 Methods

With this geometry and the Hamiltonian, I could then study the physics using a determinant quantum Monte Carlo framework called QUEST (QUantum Electron Simulation Toolbox) [9]. The sites on the lattice were numbered according tables detailing which sites were bonded to each other. I plotted the two separate crystals in Fig. 8a and Fig. 8b, to disentangle the two lattices in Fig. 1. Then I used Cartesian coordinates to produce these plots in the geometry file for QUEST. To show the bipartiteness of the lattice, the two different sublattices composing each quasicrystal in Fig. 8 are shown with blue and green colors. The nearest neighbor tables were connected with periodic boundary conditions, but these periodic boundary conditions produced a lattice that was not bipartite anymore, as can be seen in Fig. 8 because the border atoms are all the same color. Normally periodic boundary conditions are used so that the smaller lattices can more easily replicate the macroscopic properties of a system. However, a non–bipartite lattice destroys the AF ordering that we were trying to study, so open boundary conditions were used to preserved the bipartiteness necessary for antiferromagnetic ordering. This means that there are some sites with $z = 1$ and $z = 2$, even though the PBC lattice had $3 \leq z \leq 8$.

(a) 41 site quasicrystal   (b) 239 site quasicrystal
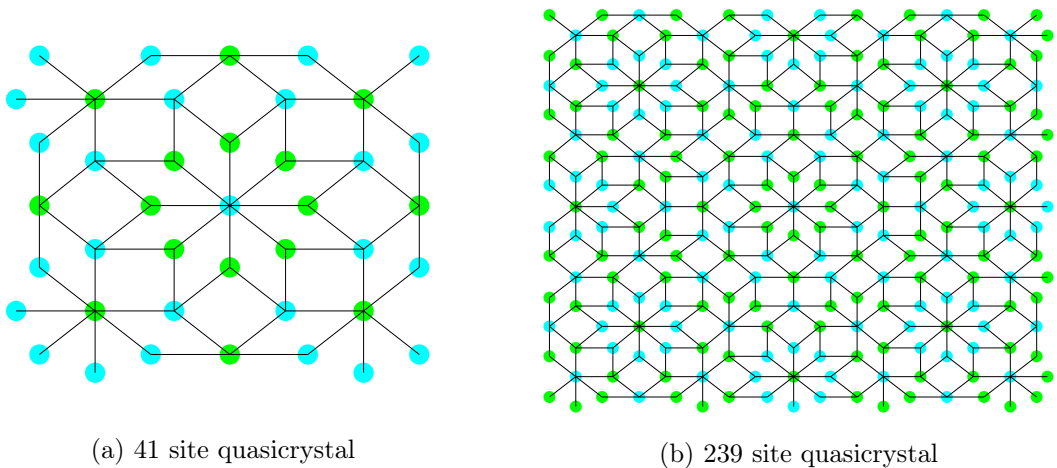
Figure 8: Illustration of how the quasicrystals lattices are bipartite

With the nearest neighbor tables, I formed matrices denoting the hoppings for 41 and 239 site quasicrystals, with dimensions 82×82, and 578×578, respectively. The eigenvalues of these matrices are easily found in Matlab, and these values can be binned into a histogram and divided by a normalization factor to generate the density of states plot, shown in Fig. 9.
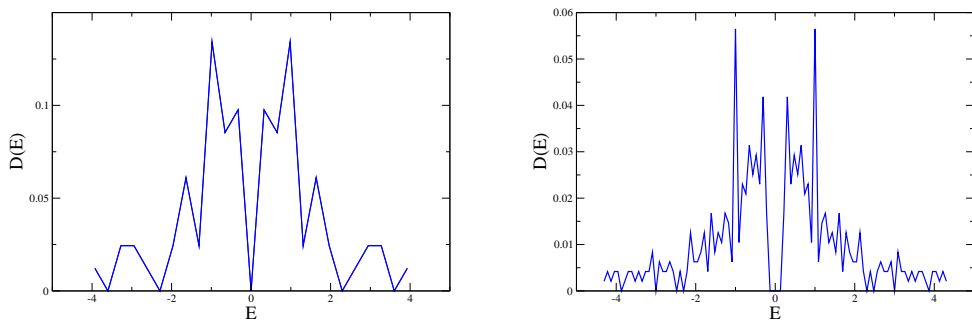
(a) 41 site quasicrystal: 82 eigenvalues binned in 25 bins

(b) 239 site quasicrystal: 478 eigenvalues binned in 100 bins

Figure 9: Density of States for the quasicrystal lattices, with $U_f = 0$

In the Hamiltonian, there are several different parameters that can be varied, t, V, U_f, and the temperature T, and this study focused on the phase transition varying only V and T, keeping t and U_f fixed at $t = 1$ and $U_f = 4$. The goal was to find V_c for the phase transition between the singlet formation and antiferromagnetic states. For this to happen, the temperature T needs to be low enough, because colder systems tend to more ordered states, according to the third law of thermodynamics. Another way we also write the temperature is $\beta = \frac{1}{T}$, in a unit system where Boltzmann's constant, k_B is 1, so absolute zero corresponds to $\beta = \infty$.

Finally, to contrast deviations in the quasicrystal from the square lattice, Prof. Scalettar ran QUEST for the Lieb lattice to compare whether a QC deviation was due to the differing coordination numbers, or the lack of periodicity.

4   Results

4.1   Quasicrystal Lattice

QUEST returns the spin-spin correlations between each of the sites, where

$$c_{ff}(i,r) = \left\langle f^\dagger_{(i+r)\downarrow} f_{(i+r)\uparrow} f^\dagger_{i\uparrow} f_{i\downarrow} \right\rangle$$

$$c_{dd}(i,r) = \left\langle d^\dagger_{(i+r)\downarrow} d_{(i+r)\uparrow} d^\dagger_{i\uparrow} d_{i\downarrow} \right\rangle \tag{4.1}$$

$$c_{fd}(i,r) = \left\langle f^\dagger_{(i+r)\downarrow} f_{(i+r)\uparrow} d^\dagger_{i\uparrow} d_{i\downarrow} \right\rangle.$$

The *singlet correlation* measures the correlation between each adjacent and localized orbital, so is defined as $c_{fd}(i, r = 0)$. Running QUEST returns a measure strength of the bond between each of the sites. So $c_{fd}(i,0) = -1$ means the d, f orbitals at site i always have *opposite* spins, $c_{fd}(i,0) = 1$ means they always have the *same* spins, and $c_{fd}(i,0) = 0$ if they are *randomly* oriented, equally likely to have the same or opposite spins. For the 41 site lattice, there are 41 different singlet correlations that we could look at. To investigate how the singlet correlation changed as a function of z, c^z_{ff} measures the average of the $c_{ff}(i,0)$ for sites with the same z.

In Fig. 10, qualitatively, we can see the 41 and 239 site lattice both demonstrate similar trends. Smaller z values tend to be more strongly correlated, which makes sense because fewer neighbors means there is less competition with the conduction sites. As $V \to 0$, $c^z_{fd}(0) \to 0$ because V is a measure of the overlap between the f and d orbitals, and if there is no overlap between the wavefunctions, the spins between these orbitals would not depend on each other. The $z = 8$ curve was omitted because we are plagued by low statistics at this point since there is only one site with this coordination number on the 41 site lattice. This graph also can also motivate a guess for V_C since this is V where the slope of the tangent line is the steepest. By taking the average of the slopes of the tangent lines for the curves $2 \le z \le 7$ for the 41 site lattice, the phase transition appears to be around $V = 0.8$. So we expect the quasicrystal at $\beta = 20$ to be in the *singlet* state when $V > 0.9$.
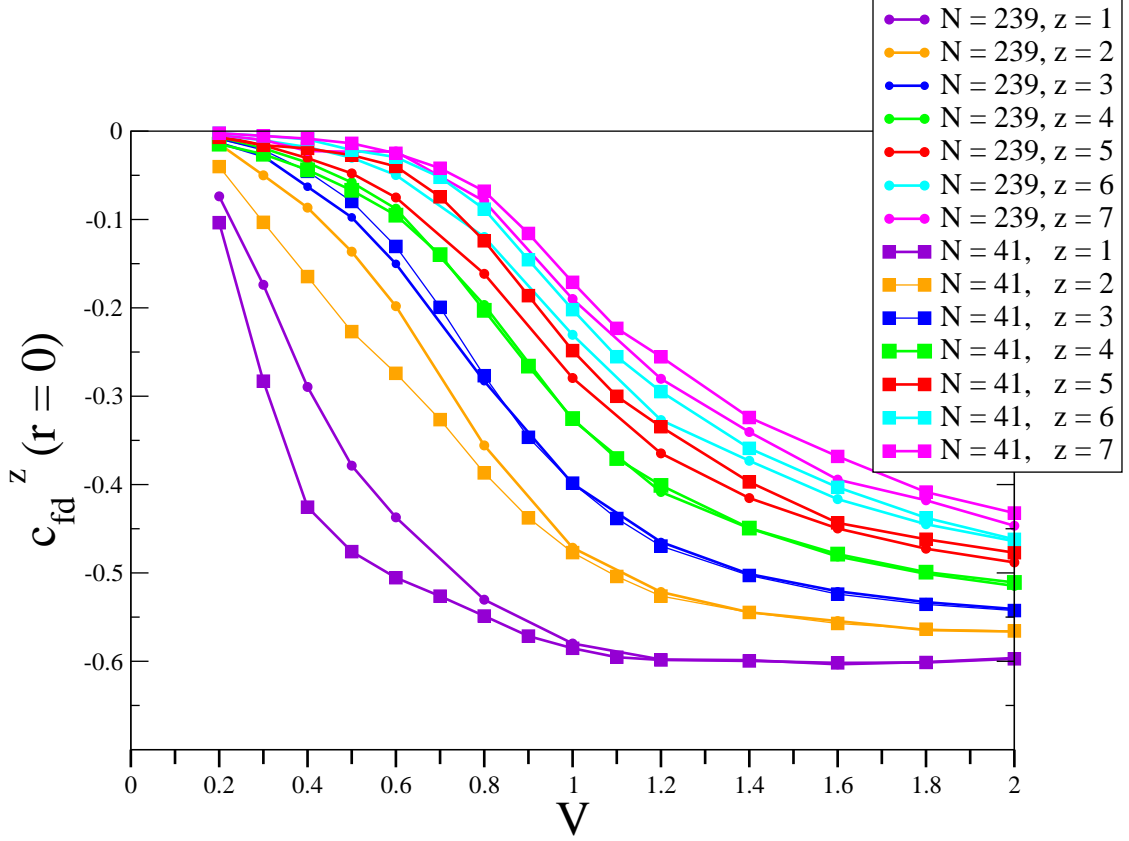
Figure 10: Singlet correlation, $c_{fd}^z(r = 0)$, $\beta = 20$

To measure the correlation between the localized orbitals, use S^{ff} defined as

$$S_{ff} = \frac{1}{N_z} \sum_i c_{ff}^z(i,r)(-1)^r \qquad (4.2)$$

which takes the average over all of the spin-spin correlations with coordination number z. N_z is the number of conduction sites that have coordination number z, so $\frac{1}{N_z}$ is the normalization factor so that $S_{ff} = 1$ if the antiferromagetic ordering is perfect. Also, $(-1)^r$ is the *phase factor*, where r is the number of hops, defined according to Fig. 11.
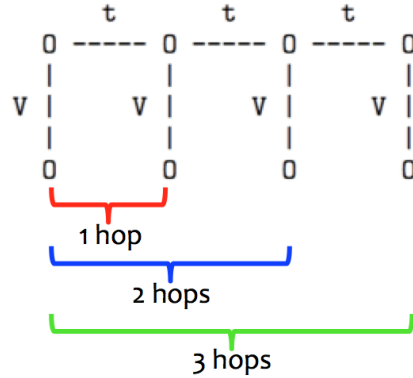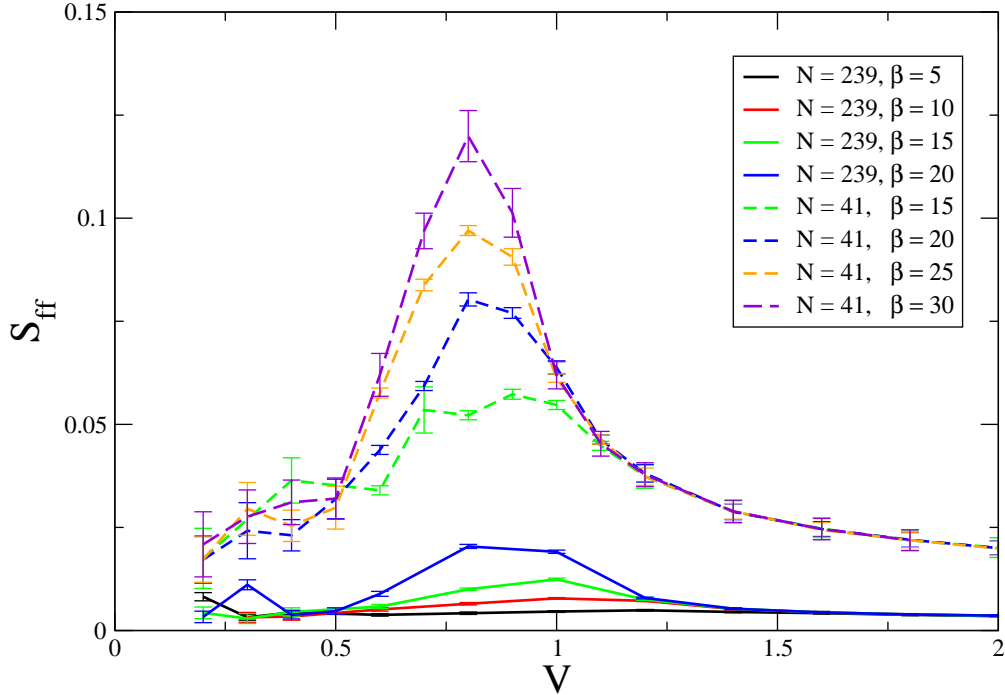

Figure 11: Illustration of how a hop is defined between localized orbitals on the lattice.

The structure factor can also be defined as a measure of the AF ordering of the lattice *independent* of the coordination number z for the individual sites,

$$S_{ff} = \frac{1}{N} \sum_i c_{ff}^z(i,r)(-1)^r \qquad (4.3)$$

where N is the number of sites on the lattice.

Figure 12: S_{ff} for the 41 and 239 site quasicrystals

In Fig. 12, the S_{ff} for the 41 and 239 site lattice is shown for a collection of β values. The 41 site crystal can be evaluated at larger β's because smaller lattices are less computationally intensive to calculate lower temperatures. S_{ff} is small for small V because less overlap between the f and d orbitals implies less "communication" between the d and f orbitals, since any electron hop between two distinct localized orbitals must first hop with an energy V to the conduction orbital, and then hop with an energy V back down to the next localized orbital. The lattice is in the ground state for large V because the curves lie directly on top of each other and the results are temperature independent. The curves appear to be peaking around $V_C = 0.8$, consistent with analysis from Fig. 10. The S_{ff} factors do not lie on top of each other, so this means that these two lattices are not large enough to replicate the macroscopic properties of the system. To test if the 239 site QC is large enough, we would need to see a larger lattice give S_{ff} values that lie on top of the 239 site curve. However, because these lattices are grown by inflation, the next sized lattice is 1339 sites [3], quite computationally expensive.

In Fig. 10 and Fig. 12 we can arrive at an approximate measure for V_C by noticing aspects of the curve, but to rigorously show whether we are in the antiferromagnetic or the singlet state, we need to plot the hopping energy as a function of the number of hops, r. Let $s^z_{ff}(r)$ be the average of the spin-spin correlation factors between a localized site whose associated conduction site has z, nearest neighbors, and another localized site r hops away. There are three possibilities for the patterning of spins in the lattice depending if we are above, at, or below the critical temperature, T_C. If $T > T_c$, $s^z_{ff}(r) = \exp\left(\frac{-r}{\xi}\right)$ and the crystal only has *short range order*, where ξ is a measure of how many hops the spin on one site can influence the spin on another. If $T = T_C$, $s^z_{ff}(r) = r^{-p}$, where p is some integer, and we are right at the phase transition. Finally, if $T < T_C$, $s^{ff}(r) = $ constant, and the crystal has a *long range order*. To have long range ordering on a finite sized lattice means that ξ is greater than or equal to the characteristic length for the lattice.
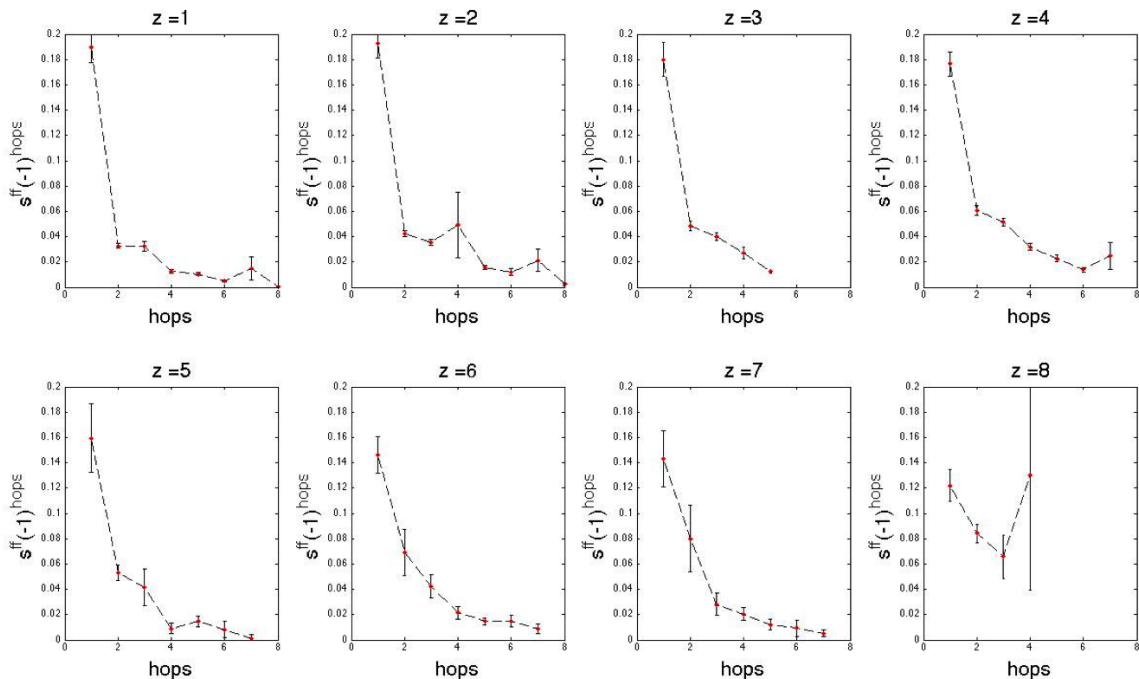
Figure 13: Singlet phase for 41 site lattice, $V = 1.0$

Consider $V = 1.0$, greater than $V_C = 0.9$, so we would expect this curve to be in the singlet phase and have short range order. In Fig. 14, the structure factors as a function of the hops are shown, but separated according to z. The curves form a zig-zag pattern, negative when the number of hops is odd, and positive when the number of hops is even, which makes sense for antiferromagnetic ordering at half-filling. The magnitude of the correlation is the largest for the smallest number of hops.

A phase factor $(-1)^{hops}$ can be included to just plot the magnitude of the structure factors, shown in Fig. 13. The curves in this subfigure appear decay exponentially, consistent with our supposition that we are in the singlet phase.

To verify this hypothesis, the $\ln\left(s^z_{ff}(-1)^{hops}\right)$ versus the hops is plotted in Fig. 15.
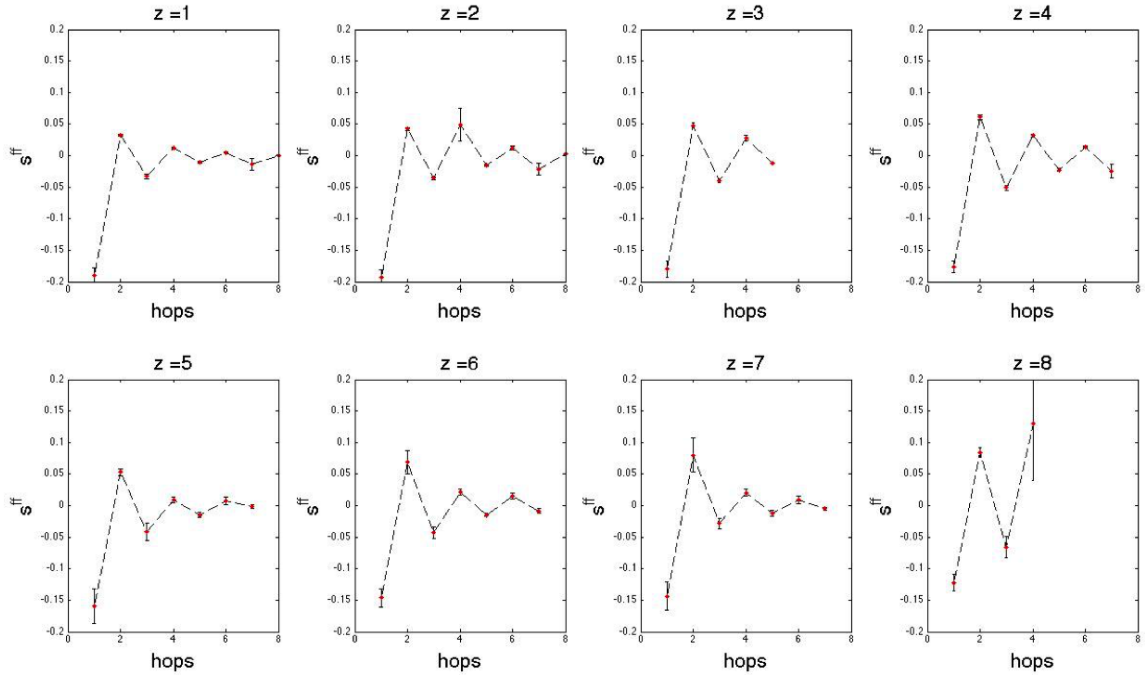
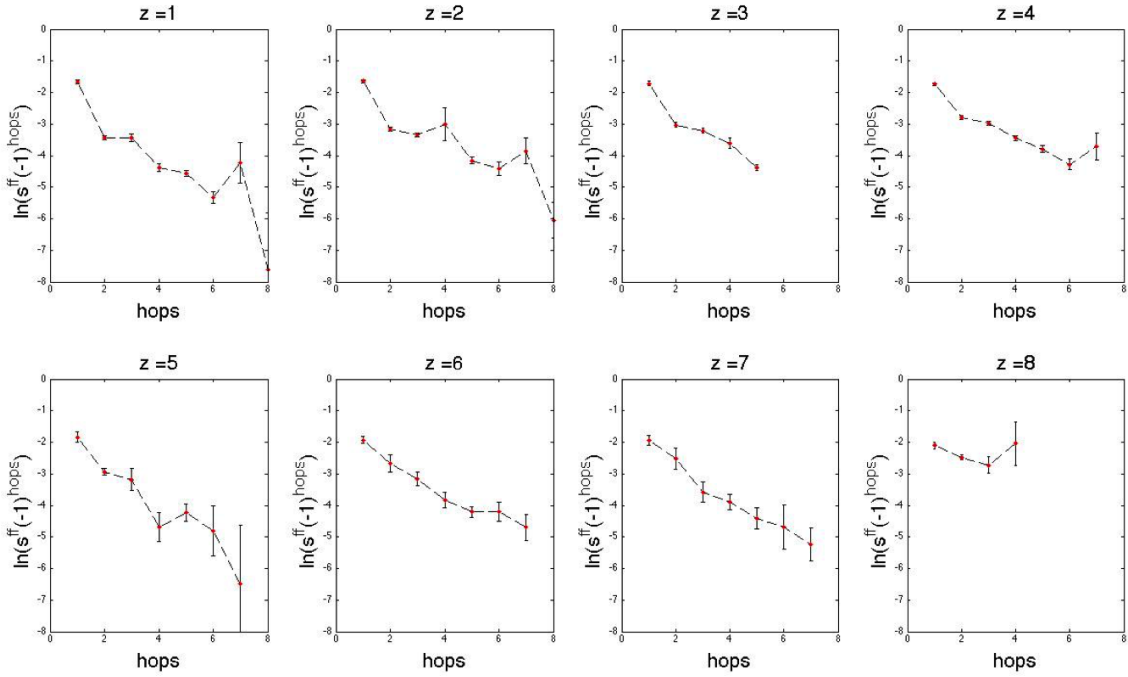**Figure 14**: Singlet phase for 41 site lattice, $V = 1.0$

Figure 15: Singlet phase for 41 site lattice, $V = 1.0$

These plots are approximately linear, which is especially obvious in the $z = 6$ and $z = 7$ cases. The slopes of these curves were calculated using a least squares fit, tabulated below.

z	Slope (a)
1	-0.613
2	-0.460
3	-0.593
4	-0.346
5	-0.672
6	-0.443
7	-0.537
8	-0.006

The slopes do not appear to follow a simple trend as a function of ξ, so to estimate ξ, just take the average of all these slopes $\langle a \rangle = -0.459$, and then $\xi = -\frac{1}{\langle a \rangle} = 2.18$. Since $\xi = 2.18 < \sqrt{41} \approx 6.4$, $V = 1.0$ has the lattice in the singlet phase with short range order.

The linearity of the $\ln\left(s_{ff}^z(r)(-1)^r\right)$ is even more dramatic for the 239 site quasicrystal, because with the greater number of sites, there are more available hops available. In Fig. 16, the $\ln\left(s_{ff}^z(r)(-1)^r\right)$ is plotted as a function of the number of hops for the different z, where the same parameters from Fig. 15 were used, $\beta = 20$ and $V = 1.0$.

A least squares fit was used to find the slopes of the lines in Fig. 16, tabulated in the table below.

z	Slope (a)
1	-0.513
2	-0.491
3	-0.481
4	-0.492
5	-0.505
6	-0.475
7	-0.543
8	-0.485

Again, the slopes do not depend on z, so the average $\langle a \rangle = -0.498$ summarizes the data from the table, and the number of hops by which one electron can influence another is $\xi = -\frac{1}{\langle a \rangle} = 2.01$, comparable to $\xi = 2.18$ from the 41 site case.

To compare the long range versus the short range order of the crystal, look at the $z = 2$ and $z = 4$ representative sites with $V = 0.8$ (in red) and $V = 1.4$ (in blue) shown in Fig. 17. While the blue square curves go to zero rapidly, the red dots continue the non-zero zig-zag pattern out to the distances allowed by the lattice, illustrating that $V = 0.8$ yields a long range order. The $z = 2, 4$ plots were shown since these correspond to the same coordination numbers from the Lieb lattice.
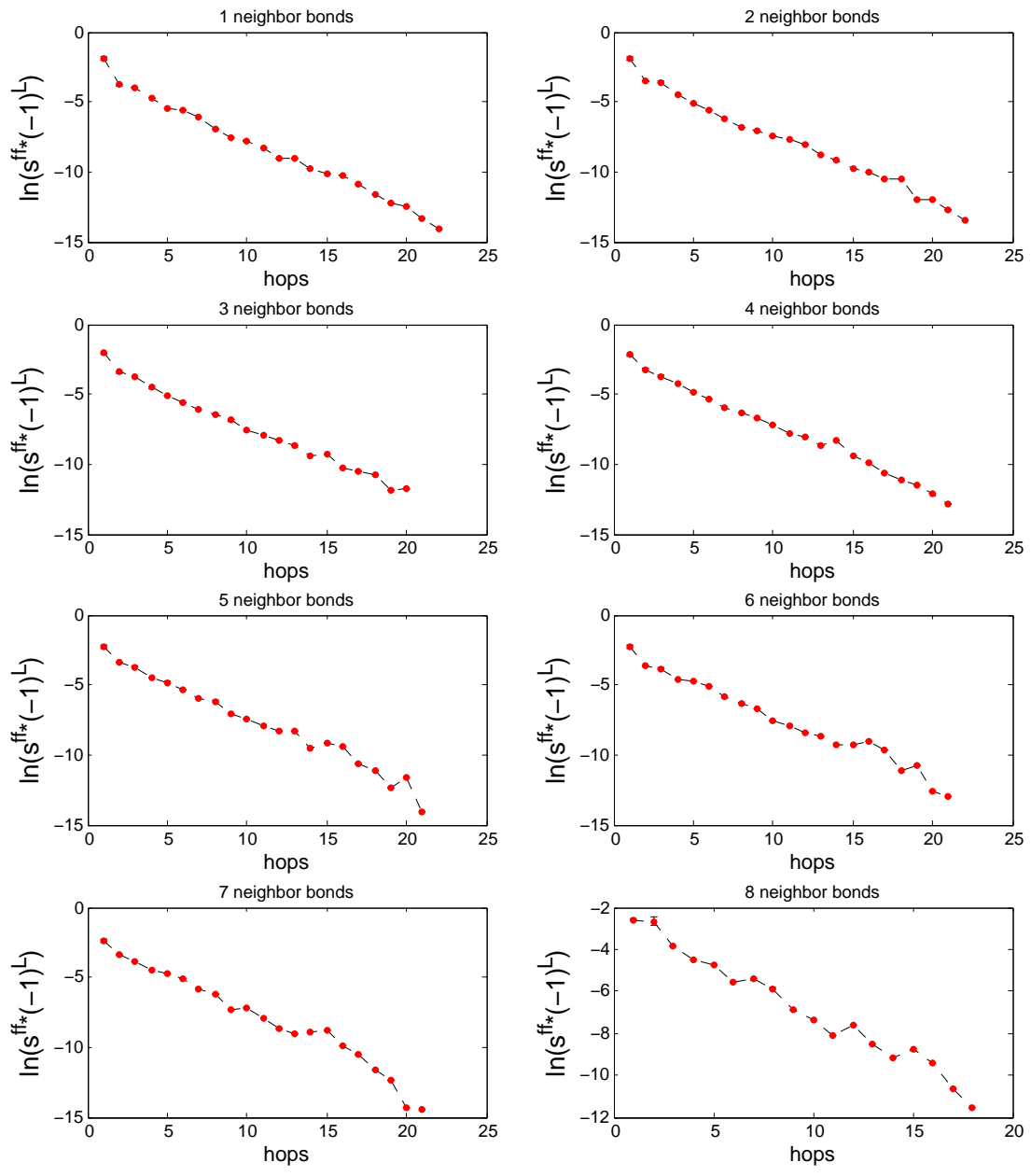
Figure 16: Singlet phase for 239 site lattice, $V = 1.0$
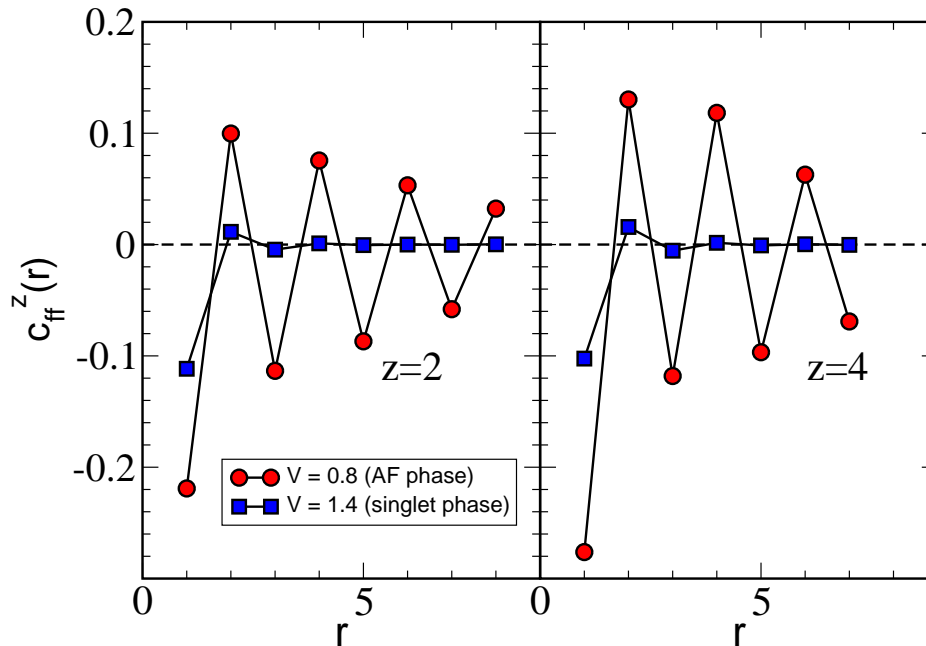
Figure 17: Comparison of the singlet vs. antiferromagnetic states as a function of V, at $\beta = 30$ for the 41 site lattice.
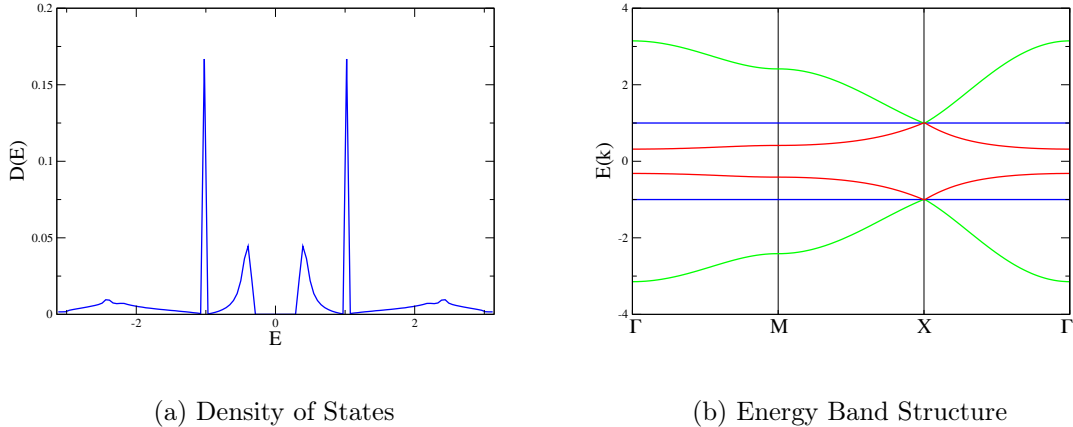
4.2 Lieb lattice

One of the advantages of the Lieb lattice is that since it is *periodic*, DQMC is not our only resort, since the density of states and energy band diagrams can be calculated by hand using the six site unit cell. The linear algebra showing the steps for the calculating the allowed energies formula is given in Section 7.3.

Then in [10], the singlet correlator, S_{ff}, and zig-zag plots for the Lieb lattice are shown.

5 Conclusions and Future Steps

Though this study, the phase transition for the quasicrystalline approximates was found to be $V_C = 0.9$. In the singlet phase ($V = 1.0$), the average number of hops from which one site can influence another is $\xi \approx 2$, and running just below at $V = 0.8$ showed long range order in the lattice. Future steps for this project might be to recreate the geometry files using a different site as the "center atoms" since it was arbitrary where periodic boundary conditions were. It would be interesting to see if the physics is preserved, or if averaging over several different geometry files could produce a more accurate answer. And of course, the program can also simply be run longer with different random number seeds to avoid getting "stuck," which could result in some unreasonable $c_{ff}(r)$ values.

(a) Density of States

(b) Energy Band Structure

Figure 18: Figures for the PAM Lieb lattice

6 Acknowledgements

7 Appendix

7.1 Additional Figures from the Quasicrystal Analysis

7.1.1 Limiting Cases Check

After encoding the geometry file, I tested a couple of limiting cases as a sanity check, shown in Fig. 19. These cases considered the self–correlation at the first conduction site, $XX_{Spin}(0,0)$ and the adjacent conduction site $XX_{Spin}(41,41)$. Because the bonds between the conduction sites are severed, we would get the same answer for any pair of adjacent f,d orbitals, and this limiting case will yield the same result for any lattice configuration. First the hopping energy V between the orbitals was tuned down to zero so that all we have is two isolated atoms, where only one has a local potential. The conduction site at (0,0) is *flat* at 0.5 as the temperature is varied, which means the spin at this site has equal probability of being up or down for any temperature. The site with a local magnetic moment at (0,0) goes to 1 as $T \to 0$, but becomes randomly oriented as the temperature is increased.

The next case in this figure has $V = 0.8$, i.e, the two site Hubbard model. At high temperature the localized and conduction site still tend to random orientations, but as the temperature is *decreased*, the hopping energy V between the conduction and valence orbitals allow the site with the potential to *induce* a magnetic moment on the other site. This causes the self–correlation for the *localized* site to fall off instead of going to 1 as before,
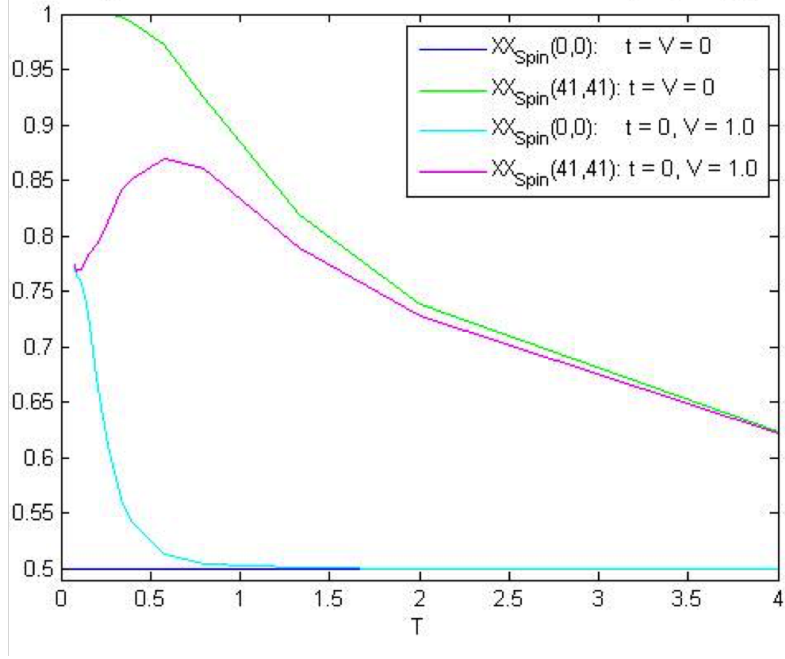
Figure 19: Limiting cases for the two-site Hubbard model with $t = 0$.

but this is similar to the process that occurs on the larger lattice as the lattice transitions to the antiferromagnetic state.

7.1.2   Comparison of Structure Factors

In Section 4, I just showed data for S_{ff} for the localized sites, but other structure factors characterizing the overlap of the *dd* and *df* orbitals as well, given by the equations below.

$$S_{dd} = \frac{1}{N} \sum_i c_{dd}^z(i, r)(-1)^r \qquad (7.1)$$

$$S_{df} = \frac{1}{N} \sum_i c_{df}^z(i, r)(-1)^r \qquad (7.2)$$

where $(-1)^r$ is the phase factor and $\frac{1}{N}$ is the normalization constant so that S_{dd} and S_{df} are 1 when the crystal has perfect antiferromagnetic order, and zero is the spins are completely randomly aligned. We could use any one of these three structure factors to characterize the AF ordering on the lattice, and Fig. 20 shows all three of these structure factors for the 41 and 239 site quasicrystals. Of the three structure factors S_{ff}, S_{dd}, and S_{df} the points on S_{ff} curve has the largest magnitude for each of the lattices, making it easier to see ordering of the lattice using this structure factor, which was why it was used in Section 4. It makes sense that S_{ff} should be the largest, because the potential well U_f was placed so that the moment formation starts at the localized sites.
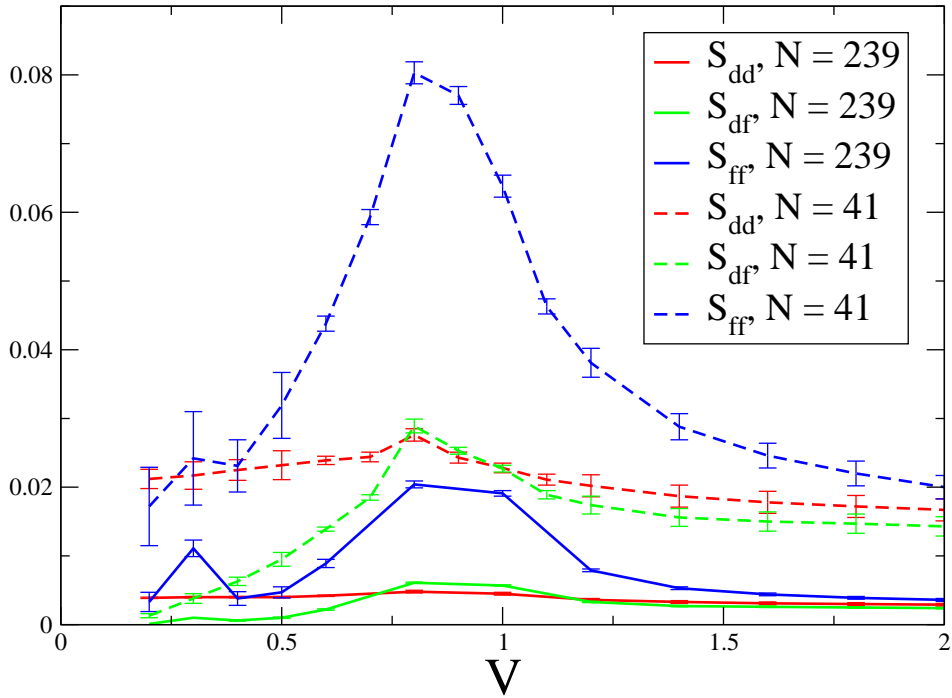
Figure 20: Structure Factors compared at $\beta = 20$.

7.1.3 Coordination Number Dependence

Then in Fig. 21a, the z dependence of the structure factor S_{ff} is shown as a function of V. For low V the errors are quite large, and is does not appear to be any ordering with respect to z values. However in the singlet phase, with the larger V values, the magnitude of the structure factor increases as the coordination number z increases.
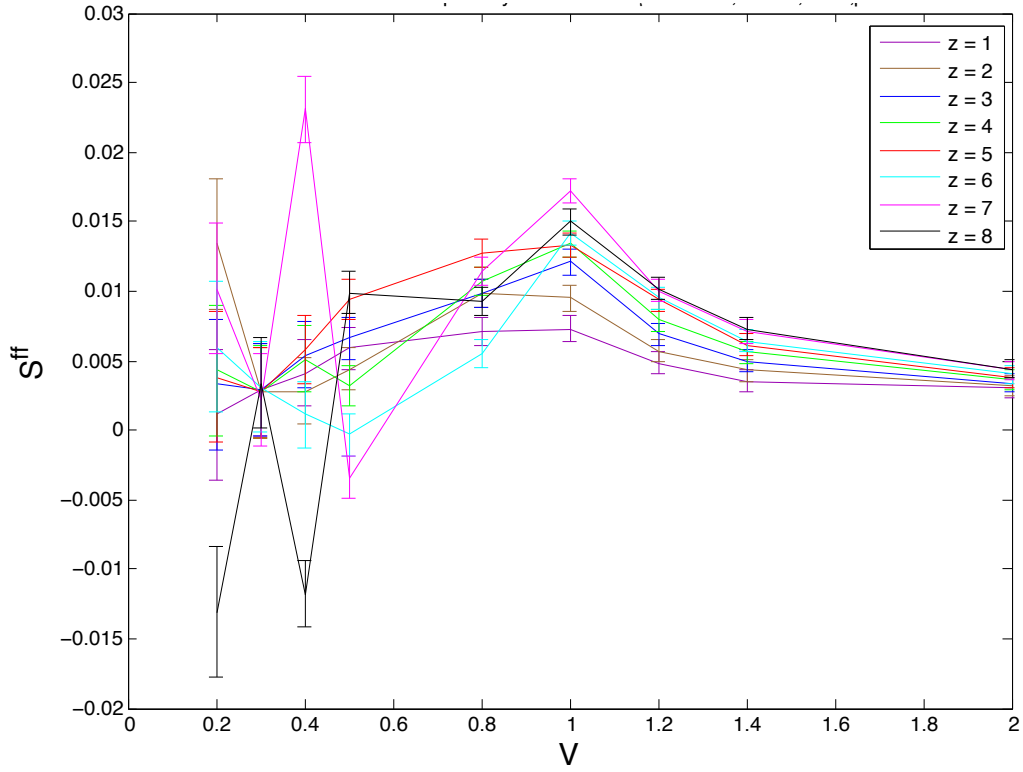
(a) z dependence of S_{ff}
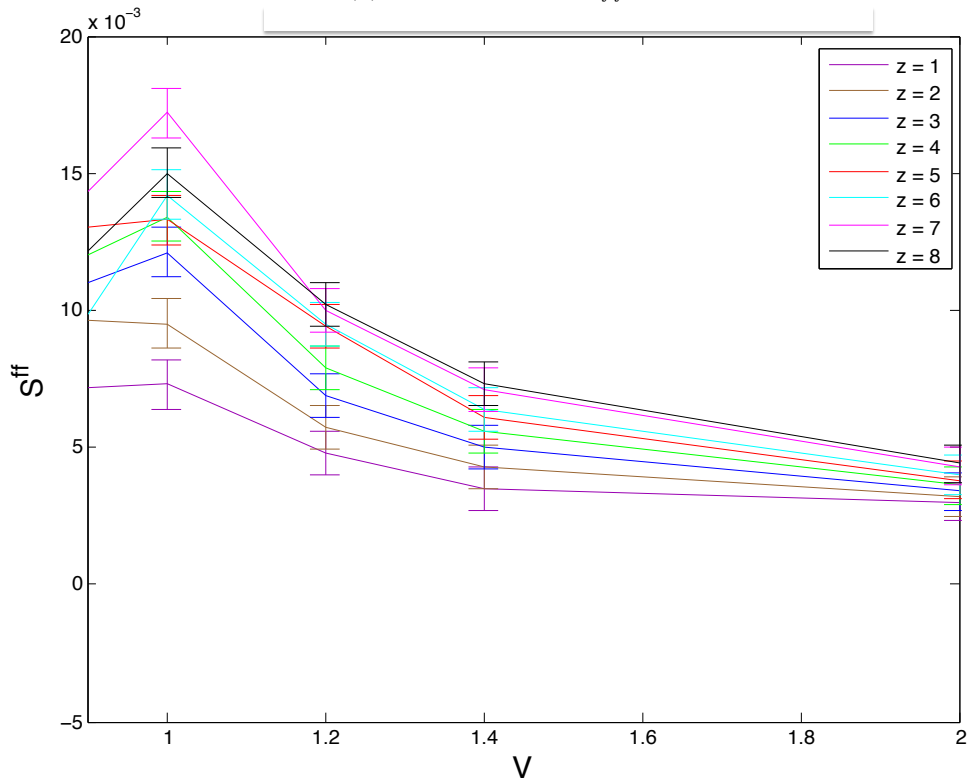
(b) Zooming in on the singlet phase

Figure 21: S_{ff}^z in the 239 site lattice at $\beta = 15$

7.2 Jackknife Errors

Some of the results for the DQMC runs had physically unreasonable values with c_{ff} larger than 1. Sometimes these were still close, like 1.34, 1.01, or 1.5, and we weren't worried about these values because since the computer only has finite precision, sometimes it will round up too much, but if it rounds down the same number of times, the average will be what it should be. However, there were sometimes a few values that were orders of magnitude too large, resulting in huge error bars.

As an example, consider a data set of spin correlations with approximately 40000 values with values around 0.1 and 10 values of 10. However, including these few 10s ludicrous values hardly affected the average which is 0.102, as it would have been 0.1 if the unphysical values were not included. This 2% hardly makes any difference, so we'd rather preserve the integrity of our scientific investigation that randomly throw out these extraneous values. Normally to find the error on a sample, we use the standard deviation from the Gaussian distribution, defined as $\sigma_{gaussian} = \sqrt{(\sum_{i=1}^{N}(x_i - \mu))/(N-1)}$, where we have N measurements of x (denoted x_i) and μ is the mean of the sample.

With the 10 $x_i = 10$ values included, $\sigma = \sqrt{\frac{10*9.9}{40010}} = 0.05$, an error 5 times as large as the vast majority of our measurements! This is because the Gaussian distribution is a smooth distribution with peaked outliers not very common. A method that can calculate the error while mitigating the effect of the errors is the jack knife method, so named because it was deemed as handy as the ubiquitous swiss army knife [11].

The Jack-Knife error is calculated in three steps:

1. Find the average μ of the sample.

2. For each x_i in the sample, calculate the sample average without the element x_i,

$$J_i = \frac{1}{N-1}\sum_{j\neq i} x_j.$$

3. Then

$$\sigma_{JK} = \sqrt{\frac{N-1}{N}\sum_{i=1}^{N}(J_i - \mu)^2} \tag{7.3}$$

Because of some outliers in the data-set, the error bars in this study were calculated using the jack-knife method. For normally distributed data, the jack-knife standard deviation returns the same result as the normal standard deviation, but for a sample with far-flung outliers, the jack-knife method provides a standard deviation closer to our intuition [11].

7.3 Density of States Calculation for the Lieb Lattice

The unit cell for the Lieb lattice has six orbitals, three conduction and three localized orbitals, as shown in Fig. 22. Once the geometry is specified, the Hamiltonian matrix for
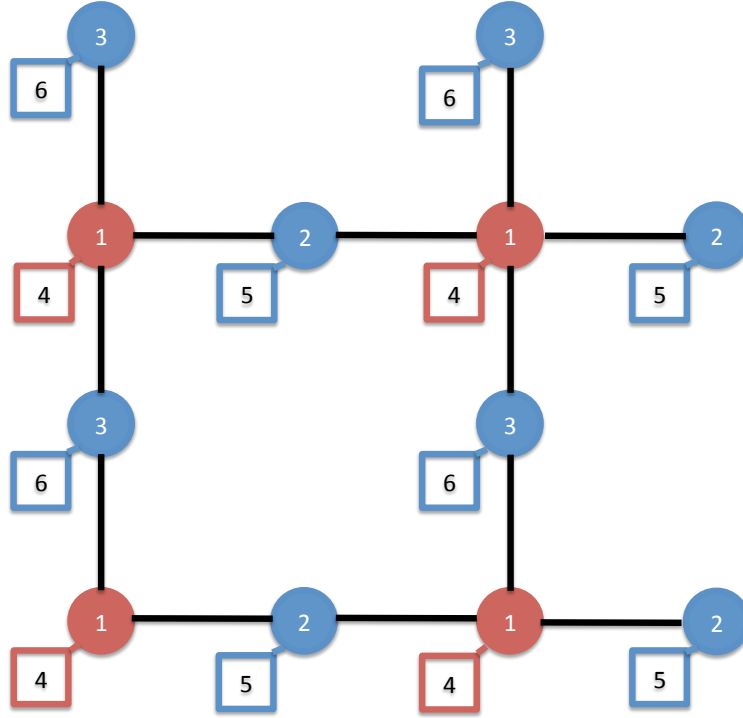
Figure 22: Lieb lattice with the numbers for the sites on the repeating unit cell. The circles represent the conduction orbitals with the solid black lines showing the nearest neighbor bonds, while the squares denote the localized orbitals. The blue circles denote the $z = 2$ sites, while the red circles denote the $z = 4$ sites., and the localized site is outlined in the same color as the adjacent conduction site to guide the eye. There are six sites in a unit cell for the adjacent Lieb lattice, and each site is numbered with a number $1 - 6$, and the pattern continues as unit cells extend to build up a larger lattice.

the system can be written down. To simplify the algebra, first solve the Hubbard model Hamiltonian with localized sites so that the unit cell consists of only 3 orbitals.

$$\hat{H} = \begin{pmatrix} 0 & -t\left(1 + e^{ik_x}\right) & -t\left(1 + e^{ik_y}\right) \\ -t\left(1 + e^{-ik_x}\right) & 0 & 0 \\ -t\left(1 + e^{-ik_y}\right) & 0 & 0 \end{pmatrix} \tag{7.4}$$

The allowed energies of the system are the eigenvalues of $\hat{H}$, and since $\hat{H}$ is a 3×3 matrix, there will be three eigenvalues. To find the eigenvalues, we need to solve the *characteristic equation*, $\left|\hat{H} - \lambda\hat{I}\right| = 0$.

$$\begin{vmatrix} -\lambda & -t\left(1 + e^{ik_x}\right) & -t\left(1 + e^{ik_y}\right) \\ -t\left(1 + e^{-ik_x}\right) & -\lambda & 0 \\ -t\left(1 + e^{-ik_y}\right) & 0 & -\lambda \end{vmatrix} = 0$$

$$\implies -\lambda^3 + \lambda t^2 \left(1 + e^{ik_x}\right)\left(1 + e^{-ik_x}\right) + \lambda t^2 \left(1 + e^{ik_y}\right)\left(1 + e^{-ik_y}\right) = 0$$

$$\implies -\lambda \left\{\lambda^2 - t^2 \left[\left(2 + e^{ik_x} + e^{-ik_x}\right) + \left(2 + e^{ik_y} + e^{-ik_y}\right)\right]\right\} = 0$$

$$\implies -\lambda \left\{\lambda^2 - t^2 \left[4 + 2\cos k_x + 2\cos k_y\right]\right\} = 0$$

$$\implies -\lambda \left(\lambda + t\sqrt{4 + 2\left(\cos k_x + \cos k_y\right)}\right)\left(\lambda - t\sqrt{4 + 2\left(\cos k_x + \cos k_y\right)}\right) = 0$$

$$\therefore \lambda = 0, \quad \pm t\sqrt{4 + 2\left(\cos k_x + \cos k_y\right)} \tag{7.5}$$

The eigenvalue $\lambda = 0$ corresponds to a *flat bland* since energy is independent of the k_x and k_y chosen. Since in the λ formula, k_x and k_y are both inside of a cosine, we will be able to calculate all of the allowed energies if we sweep k_x and k_y uniformly between 0 and π. The DOS plot for this simpler 3–site lattice is shown in Fig. 23. The spike at $E = 0$ matches the flat band at $\lambda = 0$.
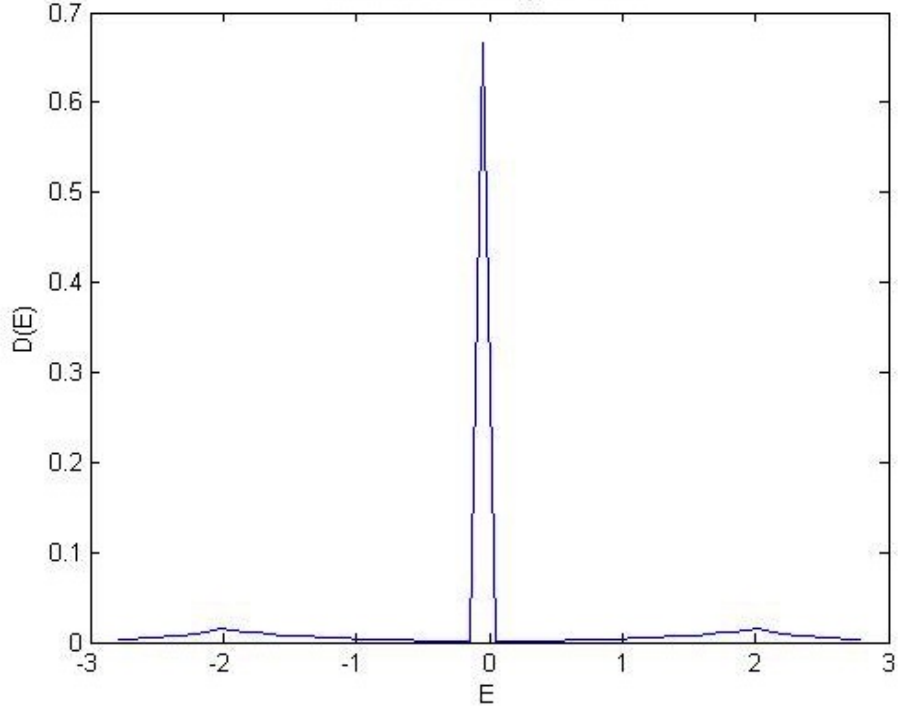
Figure 23: Density of States for the Lieb lattice with the three site unit cell.

Now consider the extension by adding the localized sites to get the PAM, with Hamiltonian

$$
\hat{H}_{PAM} = \begin{pmatrix}
0 & -t\left(1+e^{ik_x}\right) & -t\left(1+e^{ik_y}\right) & V & 0 & 0 \\
-t\left(1+e^{-ik_x}\right) & 0 & 0 & 0 & V & 0 \\
-t\left(1+e^{-ik_y}\right) & 0 & 0 & 0 & 0 & V \\
V & 0 & 0 & 0 & 0 & 0 \\
0 & V & 0 & 0 & 0 & 0 \\
0 & 0 & V & 0 & 0 & 0
\end{pmatrix}
\tag{7.6}
$$

where the upper right corner of $\hat{H}_{PAM}$ is the matrix $\hat{H}$. Now that $\hat{H}_{PAM}$ is a 6×6 matrix, there will be six eigenvalues found by solving $\left|\hat{H}_{PAM} - \lambda\hat{I}\right| = 0$.

$$
\implies \begin{vmatrix}
-\lambda & -t\left(1+e^{ik_x}\right) & -t\left(1+e^{ik_y}\right) & V & 0 & 0 \\
-t\left(1+e^{-ik_x}\right) & -\lambda & 0 & 0 & V & 0 \\
-t\left(1+e^{-ik_y}\right) & 0 & -\lambda & 0 & 0 & V \\
V & 0 & 0 & -\lambda & 0 & 0 \\
0 & V & 0 & 0 & -\lambda & 0 \\
0 & 0 & V & 0 & 0 & -\lambda
\end{vmatrix} = 0
$$

$$
\implies -V \begin{vmatrix}
-\lambda & -t\left(1+e^{ik_x}\right) & -t\left(1+e^{ik_y}\right) & V & 0 \\
-t\left(1+e^{-ik_x}\right) & -\lambda & 0 & 0 & V \\
V & 0 & 0 & -\lambda & 0 \\
0 & V & 0 & 0 & -\lambda \\
0 & 0 & V & 0 & 0
\end{vmatrix} -\lambda \begin{vmatrix}
\left(\hat{H}-\lambda\hat{I}\right) & V & 0 \\
 & 0 & V \\
 & 0 & 0 \\
V & 0 & 0 & -\lambda & 0 \\
0 & V & 0 & 0 & -\lambda
\end{vmatrix} = 0
$$

$$
\implies -V^2 \begin{vmatrix}
-\lambda & -t\left(1+e^{ik_x}\right) & V & 0 \\
-t\left(1+e^{-ik_x}\right) & -\lambda & 0 & V \\
V & 0 & -\lambda & 0 \\
0 & V & 0 & -\lambda
\end{vmatrix} + \lambda V \begin{vmatrix}
-\lambda & -t\left(1+e^{ik_x}\right) & -t\left(1+e^{ik_y}\right) & V \\
-t\left(1+e^{-ik_x}\right) & -\lambda & 0 & 0 \\
V & 0 & 0 & -\lambda \\
0 & V & 0 & 0
\end{vmatrix}
$$

$$
+ \lambda^2 \begin{vmatrix}
\left(\hat{H}-\lambda\hat{I}\right) & V \\
 & 0 \\
 & 0 \\
V & 0 & 0 & -\lambda
\end{vmatrix} = 0
$$

$$
\implies -V^3 \begin{vmatrix}
-\lambda & -t\left(1+e^{ik_x}\right) & V \\
V & 0 & -\lambda \\
0 & V & 0
\end{vmatrix} + \lambda V^2 \begin{vmatrix}
-\lambda & -t\left(1+e^{ik_x}\right) & V \\
-t\left(1+e^{-ik_x}\right) & -\lambda & 0 \\
V & 0 & -\lambda
\end{vmatrix}
$$

$$
+ \lambda V^2 \begin{vmatrix}
-\lambda & -t\left(1+e^{ik_y}\right) & V \\
-t\left(1+e^{-ik_x}\right) & 0 & 0 \\
V & 0 & -\lambda
\end{vmatrix} - \lambda^2 V \begin{vmatrix}
-t\left(1+e^{-ik_x}\right) & -\lambda & 0 \\
-t\left(1+e^{-ik_y}\right) & 0 & -\lambda \\
V & 0 & 0
\end{vmatrix} - \lambda^3 \left|\left(\hat{H}-\lambda\hat{I}\right)\right| = 0
$$

– 24 –

$$\implies V^4 \begin{vmatrix} -\lambda & V \\ V & -\lambda \end{vmatrix} \lambda V^2 \left(\lambda V^2 - \lambda \begin{vmatrix} -\lambda & -t\left(1+e^{ik_x}\right) \\ -t\left(1+e^{-ik_x}\right) & -\lambda \end{vmatrix} + \lambda V^2 - \lambda \begin{vmatrix} -\lambda & -t\left(1+e^{ik_y}\right) \\ -t\left(1+e^{-ik_x}\right) & 0 \end{vmatrix} \right)$$
$$- \lambda^4 V^2 - \lambda^3 \left| \left(\hat{H} - \lambda \hat{I} \right) \right| = 0$$

$$\implies V^4(\lambda^2 - V^2) + \lambda^2 V^4 - \lambda^2 V^2 \left[\lambda^2 - t^2(2 + 2\cos k_x) \right] + \lambda^2 V^4 - \lambda^2 V^2 [\lambda^2 - t^2(2 + 2\cos k_y)]$$
$$- \lambda^4 V^2 + \lambda^4 \left\{ \lambda^2 - t^2[4 + 2\cos k_x + 2\cos k_y] \right\} = 0$$

$$\implies V^4(\lambda^2 - V^2) + 2\lambda^2 V^4 - 2\lambda^4 V^2 - 2\lambda^2 V^2 t^2 \left(2 + \cos k_x + \cos k_y \right)$$
$$- \lambda^4 V^2 + \lambda^4 \left[\lambda^2 - t^2 \left(4 + 2\cos k_x + 2\cos k_y \right) \right] = 0$$

$$\implies V^4(\lambda^2 - V^2) - V^2 \left\{ \lambda^4 - 2\lambda^2 \left[t^2 \left(2 + \cos k_x + \cos k_y \right) + V^2 \right] \right\}$$
$$+ \lambda^2 \left\{ \lambda^4 - 2\lambda^2 \left[t^2 \left(2 + \cos k_x + \cos k_y \right) + V^2 \right] \right\} = 0$$

$$\implies \left(\lambda^2 - V^2 \right) \left\{ \lambda^4 - 2\lambda^2 \left[t^2 \left(2 + \cos k_x + \cos k_y \right) + V^2 \right] + V^4 \right\} = 0$$

The first two eigenvalues are $\lambda = \pm V$, and to find the last four eigenvalues, use the quadratic formula to solve for λ^2.

$$\lambda^4 - 2\lambda^2 \left[t^2 \left(2 + \cos k_x + \cos k_y \right) + V^2 \right] + V^4 = 0$$

$$\therefore \lambda^2 = \left[t^2 \left(2 + \cos k_x + \cos k_y \right) + V^2 \right] \pm \sqrt{\left[t^2 \left(2 + \cos k_x + \cos k_y \right) + V^2 \right]^2 - V^4}$$
$$= \left[t^2 \left(2 + \cos k_x + \cos k_y \right) + V^2 \right] \pm \sqrt{t^4 \left(2 + \cos k_x + \cos k_y \right)^2 + 2t^2 V^2 \left(2 + \cos k_x + \cos k_y \right)}$$
$$\tag{7.7}$$

In the limit $V \to 0$, Eq. (7.7) reduces to Eq. (7.5), which makes sense becuase when $V = 0$, there is no connection between the conduction and localized orbitals and all that is left is the lattice with only conduction sites. To find the density of states (DOS) loop over the allowed k_x and k_y for the system, calculate the energies, and then create a binned histogram, shown in Fig. 18a.

Finally, from this ground work, we can also plot the energy bands for the system. The plot is divided into three (k_x, k_y)
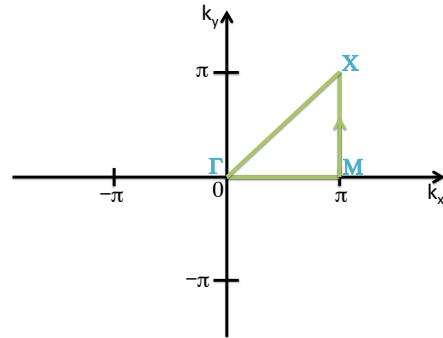
Figure 24: Triange traversed in k–space to draw the energy band diagram.

points. Γ corresponds to $(0,0)$, M is $(\pi, 0)$,
amd X is (π, π), and the six curves show how each of the eigenvalues evolves as you traverse the triangle through these points in k–*space*, illustrated in Fig. 24. Figure 18b has two flat bands at $\pm V$, because these are the only two eigenvalues that are independent of k_x and k_y.

References

[1] Kazuhiko Deguchi, Shuya Matsukawa, Noriaki K. Sato, Taisuke Hattori, Kenji Ishida, Hiroyuki Takahura, and Tsutomu Ishimasa. "Quantum critical state in a magnetic quasicrystal" *Nature Materials,* 3432,1038 (2012).

[2] Stefan Wessel, Anuradha Jagannathan, and Stephan Haas. Phys. Rev. 90, 177205 (2003).

[3] Stefan Wessel and Igor Milat. Phys. Rev. B71, 104427 (2005).

[4] Carey Huscroft, A. K. McMahan, and R. T. Scalettar. Phys. Rev. 82, 2342 (1999).

[5] Eric C. Andrade, Anuradha Jagannathan, Eduardo Miranda, Matthias Vojta, Vladimir Dobrosavljevic, Phys. Rev. Lett. 115, 03603 (2015).

[6] Richard Scalettar. "Elementary Introduction to the Hubbard Model."

[7] "Quantum physics of solids." *http://www.met.reading.ac.uk/pplato2/h-flap/phys11_4.html* Accessed 13 Aug 2015.

[8] David J. Griffiths. *Introduction to Quantum Mechanics, 2nd Ed..* Pearson Ed. Inc. (2005).

[9] QUEST: QUantum Electron Simulation. *http://quest.ucdavis.edu/index.html.* Accessed 31 Dec 2015.

[10] N. Hartman, W. T. Chiu, and R. T. Scalettar. "Magnetic Correlations in a Periodic Anderson Model with Non-Uniform Conduction Electron Coordination." (Planned for publication.)

[11] Herve Abdi, Lynne J. Williams. "Jackknife." *Encyclopedia of Research Design* (2010).